Zinc oxide nanoparticles provide anti-cholera activity by disrupting the interaction of cholera toxin with the human GM1 receptor

Received for publication, April 25, 2017, and in revised form, September 4, 2017 Published, Papers in Press, September 7, 2017, DOI 10.1074/jbc.M117.793240

Shamila Sarwar[‡1,2], **Asif Ali**[§2], **Mahadeb Pal**[§], **and Pinak Chakrabarti**[‡3]

From the [‡]*Department of Biochemistry and* [§]*Division of Molecular Medicine, Bose Institute, P1/12 CIT Scheme VIIM, Kolkata, India*

Edited by Chris Whitfield

Vibrio cholerae **causes cholera and is the leading cause of diarrhea in developing countries, highlighting the need for the development of new treatment strategies to combat this disease agent. While exploring the possibility of using zinc oxide (ZnO) nanoparticles (NPs) in cholera treatment, we previously found that ZnO NPs reduce fluid accumulation in mouse ileum induced by the cholera toxin (CT) protein. To uncover the mechanism of action of ZnO NPs on CT activity, here we used classical (O395) and El Tor (C6706)** ***V. cholerae*** **biotypes in growth and biochemical assays. We found that a ZnO NP concentration of 10 μg/ml did not affect the growth rates of these two strains, nor did we observe that ZnO NPs reduce the expression levels of CT mRNA and protein. It was observed that ZnO NPs form a complex with CT, appear to disrupt the CT secondary structure, and block its interaction with the GM1 ganglioside receptor in the outer leaflet of the plasma membrane in intestinal (HT-29) cells and thereby reduce CT uptake into the cells. In the range of 2.5–10 μg/ml, ZnO NPs exhibited no cytotoxicity on kidney (HEK293) and HT-29 cells. We conclude that ZnO NPs prevent the first step in the translocation of cholera toxin into intestinal epithelial cells without exerting measurable toxic effects on HEK293 and HT-29 cells.**

In 2015, the WHO reported 172,454 cases and 1340 deaths in 42 countries due to cholera (1); the impact of this is enormous on society (2). Cholera, an acute diarrheal disease, lethal if left untreated, is caused by the intestinal infection of *Vibrio cholerae* (3). Of more than 200 "O" serogroups, only O1 and O139 are responsible for cholera epidemics. Serogroup O1 has been classified into two biotypes, classical (Cl) and El Tor (ET), the latter is associated with the ongoing 7th pandemic first reported in 1961 (4, 5). It affects mostly places with poor sanitation resources (6), highly populated areas (7), war affected regions (8), and famine-struck territories (9). When contaminated foods or water are consumed, *V. cholerae* that has survived the acidic pH of the stomach colonizes the lining of the intestinal wall secreting cholera toxin (CT),[4] an AB5 type of toxin (10, 11). Rapid onset of vomiting with profuse rice water stools leading to the dehydration and the hypovolemic shock mostly contributes the severity of cholera (www.mayoclinic.org/diseases-conditions/cholera/symptoms-causes/dxc-20311185).[5]

Presently, the key management of cholera is the oral rehydration solution (ORS) (13)(Global Task Force on Cholera Control (2010) First steps for managing an outbreak of acute diarrhoea. *World Health Org.*).[5] It reduces the rate of mortality but it cannot reduce the duration of illness (15). So, antibiotics are recommended for severely ill patients (16). But WHO does not recommend the general use of antibiotics (17) (www.who.int/cholera/prevention_control/recommendations/en)[5] because (i) *V. cholerae* possesses a unique property of genetic plasticity (*i.e.* exchange of mobile genetic elements and genomic islands) through which several variants of *V. cholerae* have emerged. (ii) Multiple drug-resistant strains are emerging at an alarming rate. Multidrug efflux pumps, spontaneous mutation in the chromosome, and horizontal gene transfer are the mechanisms employed by *V. cholerae* for developing genetic resistance. (iii) *V. cholerae* has the potential to acquire antibiotic resistance genes from resistant bacteria and can also share with other bacteria through mobile genetic elements. In the human gut, *V. cholerae* may share this gene with other enteric pathogens and in the process may complicate the treatment for an array of infections (19). These conditions necessitate the finding of a new therapeutic strategy for the proper management of the disease.

Recently, nanoparticles (NPs) are gaining popularity as an alternative to antibiotics (20–22). Unlike antibiotics that act on specific target, NPs destroy pathogens via direct contact with the bacteria cell wall and thus bacteria are less likely to develop resistance to NPs (23, 24). Out of several NPs, we had chosen ZnO NP for studying its anti-cholera activity. The World Health Organization recommends oral zinc combined with ORS as an effective therapy to decrease the morbidity and mor-

This work was supported in part by the Department of Science and Technology, India, and the Council of Scientific and Industrial Research, India. The authors declare that they have no conflicts of interest with the contents of this article.

This article contains supplemental Figs. S1–S9.

[1] To whom correspondence may be addressed. E-mail: shamilabmb@gmail.com.

[2] Recipients of fellowships from the Council of Scientific and Industrial Research (CSIR), India.

[3] JC Bose National Fellow, India. To whom correspondence may be addressed. Tel.: 91-33-2569-3253; E-mail: pinak@jcbose.ac.in.

[4] The abbreviations used are: CT, cholera toxin; ORS, oral rehydration solution; NP, nanoparticle; HSA, human serum albumin; MTT, 3-(4,5-dimethylthiazol-2-yl)-2,5-diphenyltetrazolium bromide; qPCR, quantitative PCR; ANOVA, analysis of variance.

[5] Please note that the JBC is not responsible for the long-term archiving and maintenance of this site or any other third party hosted site.

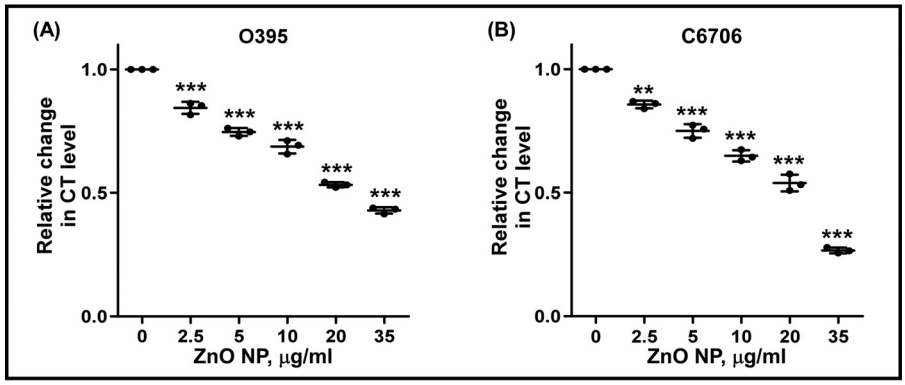

Figure 1. Determination of secreted CT levels in the CT-induced culture supernatants of (*A*) O395 and (*B*) C6706 strains, grown alone and in the presence of ZnO NP (0–35 μg/ml) by a GM1 ganglioside-based ELISA. A value of 1 indicates no change relative to control. Data were analyzed using one-way ANOVA with Dunnett's multiple comparison test. **, $p < 0.01$; ***, $p < 0.001$, $n = 3$.

tality associated with cholera (26) (www.who.int/maternal_child_adolescent/documents/9241594217/en/).[5] However, there are reports saying adding zinc to ORS did not reduce total stool output, recovery time, or disease duration (27, 28). Hence we employed ZnO NP in our study. Nano-sized particles can easily penetrate into cells and can interact with biological molecules within or on the cell surface. Furthermore, NP possess a larger surface to volume ratio that enables better interaction with biomolecules (29). Apart from that, ZnO NP has excellent stability and long shelf life (30). Recent studies have shown that ZnO NP exhibits minimal effects on human cells and have selective toxicity to bacteria (31). Our previous work (32) demonstrated the antibacterial activity of ZnO NP against *V. cholerae*. In this work, we had induced the fluid accumulation in mice ileal loop using CT, which was alleviated using the NPs. This raises the question, how did ZnO NP achieves this? Here, we have examined the action of ZnO NP on CT production by *V. cholerae* and the mechanism by which it inhibits its activity.

Results

Characterization of ZnO NP

ZnO NP was characterized using dynamic light scattering (DLS) and X-ray diffraction. The diffraction pattern obtained from X-ray diffraction (supplemental Fig. S1) is identical to that obtained from the hexagonal wurtzite phase of ZnO. Supplemental Fig. S2 represents the particle size distribution of ZnO NP as obtained from DLS, which shows that the hydrodynamic diameter of ZnO NP is 83.29 nm (Z-average diameter = 68.24 nm).

Deterioration of CT binding to GM1 after ZnO NP treatment

To observe the effect of ZnO NP on CT production by two biotypes of *V. cholerae*, we selected O395 (Cl) and C6706 (ET) strains. We explored the classical GM1 ganglioside-based ELISA for detecting the secreted CT level in the supernatant of the culture grown alone and in the presence of ZnO NP (0–50 μg/ml) under CT-induced conditions. It was observed that the level of detectable CT gets reduced by ZnO NP in a dose-dependent manner. In both the strains, the percentage of detectable CT was reduced to 50–57% at a concentration of 20 μg/ml of ZnO NP (Fig. 1). This could result from either (i) the growth inhibition of *V. cholerae* or suppression of CT production by ZnO NP, or (ii) ZnO NP interaction either with GM1 or CT and prevention of CT-GM1 binding.

Effect of ZnO NP on bacterial growth

To test the above hypotheses, we first looked upon the growth kinetics of *V. cholerae* without and with various concentrations of ZnO NP. Surprisingly, neither strain showed any significant reduction in growth up to 10 μg/ml of ZnO NP (Fig. 2, *A* and *B*); although we had observed a prominent reduction of ~40% in the level of detectable CT (Fig. 1). We also checked the impact of ZnO NP (10 μg/ml) on the bacterial membrane by monitoring the change in membrane fluidity and membrane potential. No significant change in the membrane structure was observed (supplemental Fig. S3) suggesting a healthy condition of *Vibrio* under the NP concentration used. Viability of the cell was also assessed by counting CFU and by MTT assay at the end of 18 h, and we confirmed that reduction of the CT level up to the ZnO NP concentration of 10 μg/ml does not correspond to the stressed condition of cells induced by ZnO NP (Fig. 2, *C* and *D*). It thus appears that ZnO NP is directly responsible for the low detectable CT in the culture supernatant.

ZnO NP does not affect CT expression at mRNA and protein level

CT production is under the control of master virulence regulator ToxT, which in turn is activated by a protein complex comprised of two pairs of inner membrane proteins, ToxRS and TcpPH. AphA and AphB proteins sense cell density, anaerobiosis, and other environmental cues and subsequently activate TcpPH (33).

The finding of a decrease in the CT level in both strains while cells are in healthy conditions made us speculate that either CT mRNA expression or CT protein production or both were altered. To validate our elucidation, we isolated total RNA from the untreated and NP-treated cells, made the cDNA to determine the amount of CT-specific cDNA using semi-quantitative and quantitative RT-PCR. These analyses revealed that CT mRNA expression in NP-treated cells was the same as that of the control, signifying no hindrance due to ZnO NP in the upstream regulatory cascade controlling the expression of CT (Fig. 3*A*).

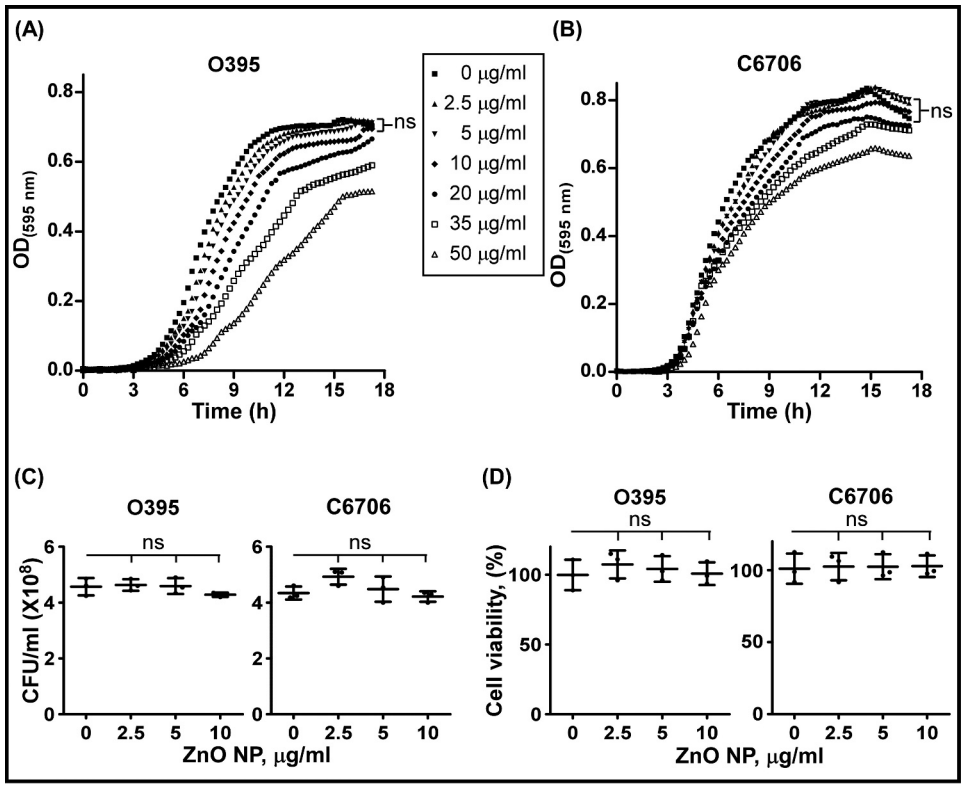

Figure 2. Effect of ZnO NP on *V. cholerae* growth. Growth curves of *V. cholerae* (*A*) O395 and (*B*) C6706 in the presence of ZnO NP (0–50 μg/ml). Viability of the cells after exposure to ZnO NP (0–10 μg/ml) for 18 h, as measured by (*C*) CFU analysis and (*D*) MTT assay. *ns* defines no statistically significant differences. All data represent the value of three independent experiments.

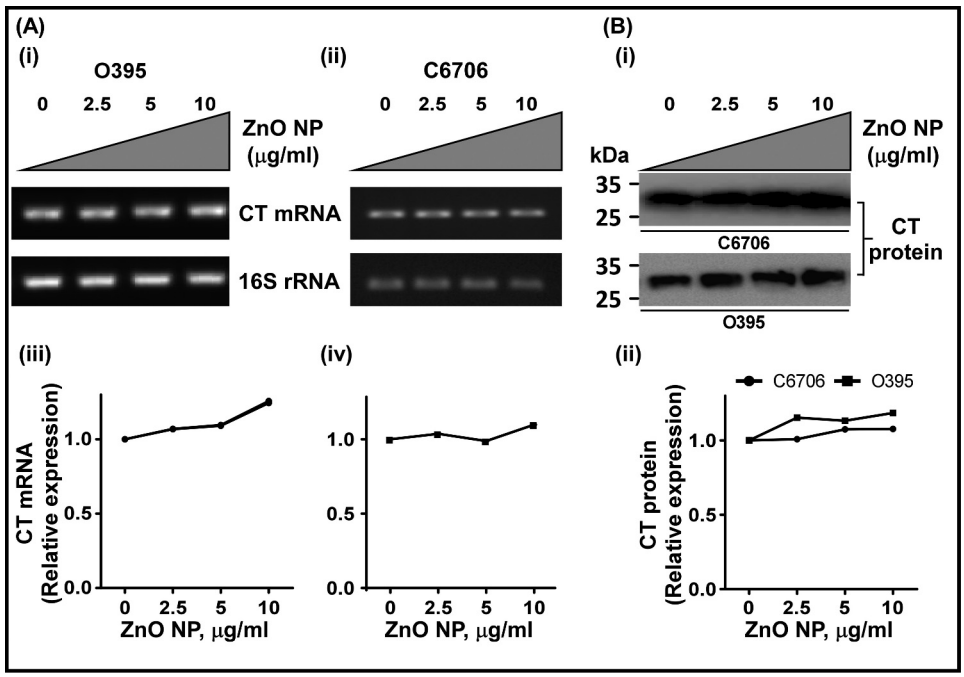

Figure 3. Effect of ZnO NP on production of CT at RNA and protein level. *A*, *panels i* and *ii,* ethidium bromide-stained agarose gels, demonstrating semi-quantitative RT-PCR data of CT mRNA and 16S rRNA (loading control) expression in *V. cholerae* treated with ZnO NP (0–10 μg/ml). *Panels iii* and *iv*, scatter plot demonstrating fold-change of CT at mRNA level by quantitative RT-PCR, normalized against 16S rRNA. *B*, *panel i*, immunoblot of CT protein present in the supernatant of the bacterial cultures cultivated in the absence and presence of ZnO NP (0–10 μg/ml), normalized against cell density. *Panel ii*, scatter plot, demonstrating the quantitation of CT protein of figure (*i*) by ImageJ software. All data represent the value of three independent experiments.

The next possibility of reduced CT protein level was examined by immunoblot analysis of untreated and NP-treated culture supernatants using anti-CT antibody. Importantly, no change in the concentration of CT protein was seen with varying concentrations of ZnO NP (Fig. 3*B*). These results annulled our first assumption that GM1 ELISA detected low CT in the

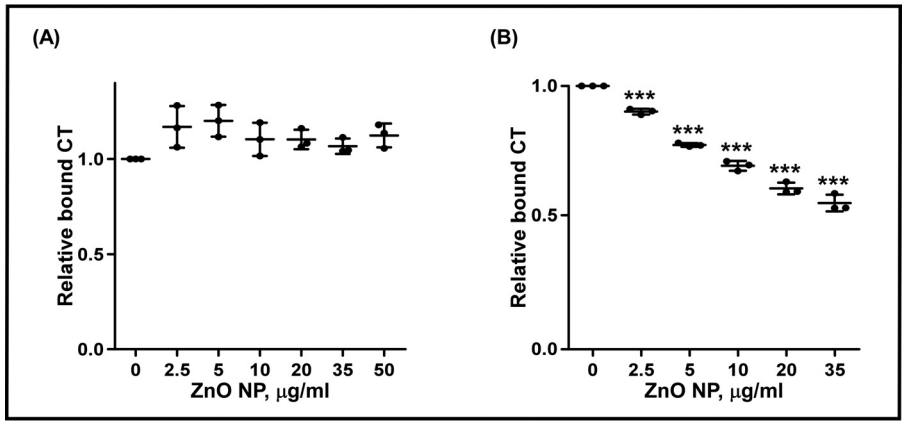

Figure 4. Effect of ZnO NP on the activity of CT by GM1 ELISA. Determination of CT level by GM1 ganglioside-based ELISA. *A,* GM1-coated wells incubated with ZnO NP (0–50 μg/ml) followed by 3 μM purified CT. *B,* GM1-coated wells incubated with 3 μM purified CT treated with ZnO NP (0–35 μg/ml). Data were analyzed using one-way ANOVA with Dunnett's multiple comparison test. ***, $p < 0.001$, $n = 3$.

presence of ZnO NP due to growth inhibition of *V. cholerae* or suppression of CT production.

ZnO NP does not interact with GM1

Because ZnO NP exhibits no effect on CT production and secretion, next we studied if ZnO NP binds to the GM1 receptor and inhibits its activity to attach with CT. We treated the GM1-coated wells with ZnO NP for 2 h, washed three times with PBS (1X) prior to its incubation with CT, followed with the standard GM1 ganglioside-based ELISA protocols. No change in CT binding to the NP-treated GM1 was observed (Fig. 4*A*), suggesting no role of GM1. However, when ELISA was performed with NP-treated CT (2 h), there was a continuous decrease in CT binding to GM1 with increasing concentrations of ZnO NP, indicating the importance of the interaction of ZnO NP with CT (Fig. 4*B*).

ZnO NP disturbs the secondary structure of CT via complex formation

The interaction of ZnO NP with CT protein was studied using biophysical techniques. Fluorescence quenching is one of the widely used processes to study the interactions between biomolecules and ligand. For quenching to occur, the fluorophore and the quencher need to be in contact with each other. The quenching may be a collisional (dynamic) or complex formation (static) (34). The intrinsic fluorescence emission of Trp of CT in the presence of different concentrations of ZnO NP is shown in Fig. 5*A*. The fluorescence intensity decreased gradually with increasing concentrations of ZnO NP with a slight red shift in the emission maxima signifying the exposure of the Trp residue to the polar environment. The linear Stern-Volmer plot of F_o/F *versus* the concentration of ZnO NP indicates the presence of only one type of quenching of CT in the presence of ZnO NP. To elucidate the molecular mechanism of CT-ZnO NP interaction, Stern-Volmer plots of F_o/F *versus* the concentration of ZnO NP were plotted for two different temperatures (18 and 45 °C). The linear plot of F_o/F_c against the concentration of ZnO NP and decreasing slope with an increase in temperature suggest the homogeneous static quenching (Fig. 5*B*).

To determine the effect of ZnO NP on the secondary and tertiary structures of CT, we performed far-UV and near-UV circular dichroism studies (35). As evident from the far-UV CD spectra given in Fig. 5*C*, there was a slight decrease in the negative ellipticity in the far-UV region of CD without any significant shift of the peak, thereby suggesting a subtle change in the α-helical content of CT in the presence of ZnO NP. Likewise, near-UV circular dichroism also did not indicate any major change in the tertiary structure of CT (supplemental Fig. S4).

To further confirm the interaction between CT protein and ZnO NP, we incubated ZnO NP with the CT-induced culture supernatant of both strains for 1 h at room temperature followed by washing with PBS. The pellet was dissolved in Laemmli buffer and was examined for CT protein that could adsorb on ZnO NP via immunoblot assay using anti-CT antibody. As revealed in Fig. 5*D* with increasing concentrations of ZnO NP, there is an enhancement of CT adsorption. Furthermore, we also used anti-HAP antibody to check for another protein in the supernatant co-pellet with ZnO NP. HAP is an extracellular metalloprotease secreted by *V. cholerae* during nutrient limitation, while entering into stationary phase and at high cell population density (36). The absence of HAP-specific bands in the ZnO NP-treated samples indicates no interaction of HAP with ZnO NP (supplemental Fig. S5*A*). We further compared the interaction of ZnO NP with the purified proteins, such as heat shock protein (HSP90α), tubulin, and CT. As shown in supplemental Fig. S5*B*, ZnO NP adsorbs CT in a concentration-dependent manner but no significant interaction was found with either HSP90α or tubulin.

To examine if ZnO NP affects the integrity of CT (AB5), the holotoxin was incubated with ZnO NP (10 μg/ml) and in 3 M urea, pH 3.5 (positive control), separately for 1 h. After incubation, gel filtration chromatography was performed. Supplemental Fig. S6*B* represents the elution patterns of CT alone, in the presence of ZnO NP and with urea, pH 3.5. The profiles demonstrate no dissociation of CT subunits in the presence of ZnO NP, whereas the urea-treated sample showed significant dissociation (positive control). Albumin (67 kDa), chymotrypsinogen A (25 kDa), and lysozyme (14.3 kDa) were used as molecular mass markers (supplemental Fig. S6*A*). We further confirmed the results by running a 7.5% native polyacrylamide gel. For positive control, CT was heat denatured

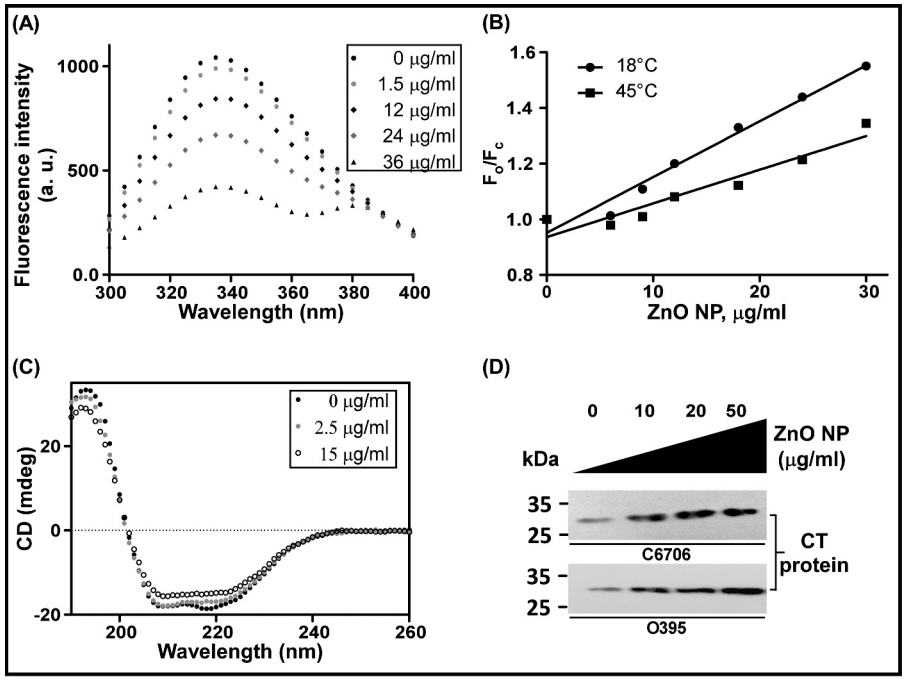

Figure 5. Evaluation of ZnO NP interaction with CT using spectroscopic methods. *A,* fluorescence emission spectra of CT (3 μM) with increasing concentrations of ZnO NP (0–36 μg/ml). *B,* Stern-Volmer plots of fluorescence quenching for CT with ZnO NP at two different temperatures (18 and 45 °C). Data shown are corrected for inner filter effect. *C,* secondary structure of native CT and CT bound to ZnO NP (0–15 μg/ml) monitored by far-UV CD spectra. *D,* estimation of CT protein adsorbed on ZnO NP by immunoblot assay.

(supplemental Fig. S7). Again, the oligomeric structure of CT seemed to have remained unchanged.

Structure and activity of some standard proteins in the presence of ZnO NP

To understand if the inhibitory activity of ZnO NP is specific to CT, we studied the specificity of four standard proteins (lysozyme, human serum albumin (HSA), HSP90α, and tubulin), the first three of which were also studied for their activity. Intrinsic Trp fluorescence quenching experiments indicate that ZnO NP does not interact with tubulin and HSP90α, whereas it binds with lysozyme and HSA at the working concentration (supplemental Fig. S8). Although interaction takes place between HSA, lysozyme, and ZnO NP, the activities of these proteins are not compromised (supplemental Fig. S9).

HT-29 cell bioassay

HT-29 is a human colorectal adenocarcinoma cell line, established in 1964 from the primary tumor of a 44-year-old Caucasian female with colorectal adenocarcinoma. This cell line is used as an *in vitro* model to study cholera toxin binding by intestinal cells. In the presence of CT, large pleomorphic vacuoles are formed in HT-29 cells (37). We utilized this bioassay to check the effectiveness of ZnO NP against biological activity of CT. HT-29 cells were treated with CT alone and NP-treated CT. The CT-induced vacuoles formation was inhibited by ZnO NP in a concentration-dependent manner emphasizing the inhibition of biological activity of CT as shown in Fig. 6*A*.

Effect of ZnO NP on CT uptake by HT-29 cells

We further investigated the effects of ZnO NP on CT uptake by cells. For this study, an immunoblot assay was done with the lysates of HT-29 cells incubated with CT and NP-treated CT. Blot analysis clearly demonstrated the fact that ZnO NP interacts with CT and does not allow its binding with GM1 present on the cell surface hence reducing its uptake by the cells (Fig. 6, *B* and *C*).

Cytotoxicity in HEK293 cells

The study of cytotoxicity of ZnO NP on the human embryonic kidney cells (HEK293) and HT-29 cells would be helpful to determine whether the concentrations of ZnO NP used in this study are non-cytotoxic. For this, HEK293 and HT-29 were treated with various concentrations (2.5, 5, and 10 μg/ml) of ZnO NP for 48 h and the percentage of viable cells were measured by MTT assay. As evident from Fig. 6*D*, ZnO NP was found to be non-toxic in the effective range of concentration.

Discussion

In our previous paper (32), we reported the detailed antibacterial activity of ZnO NP (~7–10 nm) against two biotypes of O1 serogroup of *V. cholerae*: classical (O395) and El Tor (N16961). We observed that ZnO NP exerts its anti-*Vibrio* activity by producing reactive oxygen species and disrupting the bacterial membrane that leads to depolarization of membrane, increased permeabilization, protein leakage, and DNA damage. We had also shown that ZnO NP effectively blocked intestinal fluid secretion induced by purified CT (32). These results prompted us to examine the mechanistic study of the anti-cholera activity of ZnO NP at a concentration (10 μg/ml) at which the bacterial cells remain unaffected.

CT initiates its pathogenic effect by binding to GM1 ganglioside receptor present on the intestinal epithelial barrier. This complex is endocytosed and transported to endoplasmic retic-

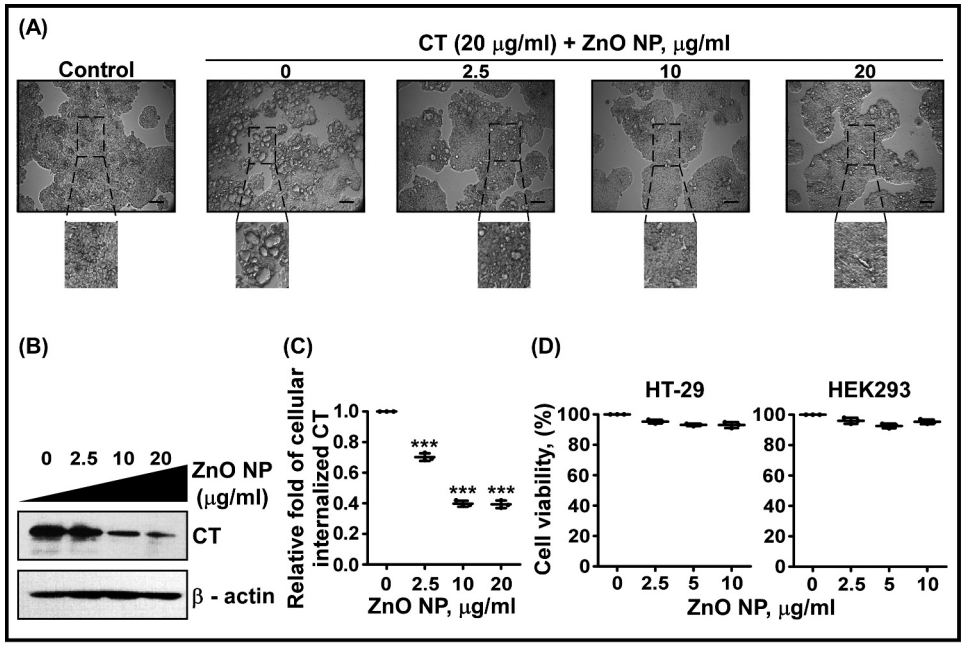

Figure 6. Uptake of CT by HT-29 cells. *A,* phase-contrast microscopic images showing that ZnO NP ameliorates vacuole formation by CT in a concentration-dependent manner (magnification, ×20; *scale bar*, 10 μm); *dashed box* indicates an enlarged view of that section. Cells with no ZnO NP or CT treatment constitute the control. *B* and *C*, level of internalized CT as determined by immunoblot from whole cell lysates of HT-29 cells; β-actin is used as the loading control. *D*, percentage of viable HT-29 and HEK293 cells after exposure to ZnO NP (0–10 μg/ml) for 48 h, as measured by MTT assay. Data were analyzed using one-way ANOVA with Dunnett's multiple comparison test. ***, $p < 0.001$, $n = 3$.

ulum for the activation of cholera toxin A subunit. The activated cholera toxin A, in turn, activates the G protein by adenosine diphosphate (ADP)-ribosylation of its $G_{\alpha s}$ subunit thereby increasing adenylate cyclase activity to produce cyclic adenosine monophosphate (cAMP). The high level of intracellular cAMP stimulates protein kinase A (PKA) to turn on the cystic fibrosis transmembrane conductance regulator, leading to the efflux of Cl^- ions followed with Na^+ ions and water, resulting in rice water stools (38).

The present management of cholera aims at recovery rather than cure. The usage of antibiotics in severely ill patients may kill bacteria but cannot inhibit the action of cholera toxin once produced. Hence, finding a drug that can kill the pathogen as well as block the activity of cholera toxin already secreted by colonized bacteria may boost the present therapeutic strategies. In literature, various compounds are reported to inhibit cholera toxin activity via different mechanisms. For example, Virstatin inhibits the transcriptional regulator ToxT, thereby preventing the expression of toxin-coregulated pilus and cholera toxin (39, 40). Plant-derived dihydroisosteviol reversibly inhibits cystic fibrosis transmembrane conductance regulator chloride channels (41). Capsaicin, one of the active compounds of red chili, acts as a repressor of CT production by enhancing the transcription of the *hns* gene coding for the histone-like nucleoid structure protein (42). In a related study gold NPs have been found to destabilize the structure of another *V. cholerae* toxin Ace, and thereby prevent fluid accumulation in mouse ileal loop (43).

In this paper, we report the anti-cholera toxin activity of ZnO NP. We showed ZnO NP binds with CT and prevents its attachment with the receptor GM1 thus inhibiting the very first crucial step of CT-induced diarrhea. To study the anti-cholera toxin activity, we selected the optimal dose at which ZnO NP is neither detrimental to *V. cholerae* nor to HEK293 and HT-29 cells. Our findings suggest that ZnO NP when added to O395 and C6706 culture supernatants brought about a decrease in the CT level as detected by ELISA (Fig. 1), although no change in CT concentration was observed by Western blot analysis (Fig. 3*B*). This was also corroborated with no alteration in the transcription of CT mRNA (Fig. 3*A*). These outcomes point toward the effect of ZnO NP on CT-GM1 binding. We further extended our study to investigate the exact mechanism of action of ZnO NP. We found no change in the CT level when GM1 was treated with different concentrations of ZnO NP, whereas CT-GM1 interactions decreased in a dose-dependent manner when CT was treated with ZnO NP (Fig. 4). We explored the CT-ZnO NP interaction by performing biophysical studies. Fluorescence study revealed a decrease in fluorescence intensities with a slight spectral red shift of 2 nm indicating unfolding of the CT secondary structure upon binding to ZnO NP (Fig. 5, *A* and *B*). Far-UV CD analysis indicated that the α-helical content of CT was reduced with the concomitant increase in random coil, when CT was treated with ZnO NP (Fig. 5*C*).

Finally, we checked the effectiveness of ZnO NP in reducing CT-induced pathological effects and CT binding on HT-29 cells. According to literature, large vacuoles are formed when HT-29 cells are incubated with CT. Our results demonstrated that NP-treated CT failed to induce vacuoles and also uptake of CT by HT-29 cells decrease in a dose-dependent manner (Fig. 6).

ZnO NP has been shown to have an antibacterial effect (32). It may be mentioned that the antibacterial effect of any NP is influenced by its size. ZnO NP used here are about 10 times

larger than the previous work (32). Although 25 μg/ml was found to disrupt the membrane structure (32), a concentration of 10 μg/ml did not affect the membrane integrity to any significant extent (supplemental Fig. S3). But even at this concentration, which is non-cytotoxic (Fig. 6*D*), and which does not inhibit the growth of *V. cholerae* (Fig. 2), it can inhibit cholera toxin activity. All these results suggest that ZnO NP has the potential for clinical application in preventing cholera infection, although further studies need to be done to translate it as a cholera treatment for human.

Experimental procedures

V. cholerae classical biotype strain O395 and El Tor strain C6706 were used in these studies. These strains were gift from Dr. R. K. Nandy (National Institute of Cholera and Enteric Diseases, Kolkata) and Dr. Rukhsana Chowdhury (Indian Institute of Chemical Biology, Kolkata), respectively, and maintained in our laboratory. CT (AB5), anti-rabbit IgG (whole molecule)–peroxidase antibody produced in goat, anti-cholera toxin antibody produced in rabbit, monosialoganglioside GM1 from bovine brain, streptomycin, and ZnO NP were purchased from Sigma. Anti-HAP antibody produced in rabbit was a gift from Dr. Amit Pal (NICED, Kolkata).

Characterization of ZnO nanoparticles

Zinc oxide, dispersion nanoparticles, <100 nm particle size, was purchased from Sigma. Prior to use, ZnO NP were characterized. Particle size was determined by the DLS technique using Zetasizer Nano ZS Malvern Instrument (Worcestershire, UK). X-ray diffraction pattern for the ZnO NPs was recorded using an X-Ray Powder Diffractometer, Rigaku MiniFlex (The Woodlands, TX), using CuKα radiation of wavelength λ = 0.1541 nm, maintaining an applied voltage of 30 kV and current at 15 mA in the scan range $2\theta = 10-80°$.

GM1 ganglioside based ELISA

Cultures of both strains (O395 and C6706) were grown under toxin-inducing conditions in the absence and presence of varying concentrations of ZnO NP. After 18 h cells were pelleted down and the supernatant was collected. To estimate the CT content, supernatants were added to GM1-coated microtiter wells and ELISA was performed (www.cdc.gov/cholera/Laboratory.html)[5] using anti-cholera toxin antibody and anti-rabbit IgG (whole molecule)–peroxidase antibody. The color intensity was measured at 450 nm in an ELISA plate reader.

Bacterial susceptibility test

From the overnight grown cultures of the respective strains, 1% was inoculated into fresh Luria-Bertani broth and grown to a turbidity of 0.5 McFarland standards. A growth inhibition study was performed under toxin-inducing conditions, 200 μl of culture (equivalent to $\sim 5 \times 10^5$ CFU) was incubated at 30 °C in the presence and absence of different concentrations of ZnO NP in a 96-well flat-bottom microtiter plate (Tarsons), and absorbance was recorded at 595 nm at every 15 min up to 18 h in a microplate reader. Cell viability was checked by plating appropriate dilution of culture onto LB plates at 18 h.

RNA isolation, semi-quantitative, and quantitative RT-PCR

For RNA isolation cells were treated as before for 18 h. Total RNA was isolated using TRIzol reagent (Invitrogen). Furthermore, the pooled RNA (600 ng) was converted to one-strand cDNA using Verso cDNA synthesis kit (Thermo Scientific) as per the manufacturer's instructions. Then semi-quantitative RT-PCR was performed using CT- and 16S rRNA-specific primers. Amplification was performed for 37 cycles (96 °C for 30 s, 55 °C for 45 s, and 72 °C for 45 s). 10 μl of each PCR product was electrophoresed on a 2% agarose gel and visualized using ethidium bromide. PCR products were normalized according to the amount of 16S rRNA detected in the same cDNA sample. The data for the mRNA transcript levels were further validated by performing quantitative-PCR (qPCR) (7500 Fast Real-time PCR system, Applied Biosystems) using 2× SYBR Green (hot jumpstart sybr green, Sigma) and a CT-specific primer. Data analysis was done according to the Livak method using 16S rRNA as an internal control.

Western blotting

Electrophoresis was carried out using the treated culture supernatants of the respective strains and transferred onto polyvinylidene difluoride membrane (Millipore). Immunoblotting was done using anti-cholera toxin antibody (1:2000) followed by incubation with anti-rabbit IgG (whole molecule)–peroxidase antibody (1:1000). The horseradish peroxidase-positive bands were visualized using Lumi-Light Western blotting substrate (Roche Applied Science) in the dark.

Fluorescence spectroscopy

The fluorescence spectrum of CT (3 μM) was studied on a PerkinElmer fluorescence spectrophotometer using a quartz cuvette with a 1-cm path length at specified temperatures. The excitation and emission spectra were set at 282 and 310 to 400 nm, respectively. For fluorescence quenching measurements, ZnO NP was added successively to CT and the final fluorescence values were corrected for the inner filter effect using the following equation (12).

$$F_{corr} = F_{obs} \times 10^{\frac{A_{ex} + A_{em}}{2}} \quad \text{(Eq. 1)}$$

Where F_{corr} and F_{obs} are the corrected and the observed fluorescence intensities, respectively, A_{ex} and A_{em} are the absorbencies of the sample at the excitation and emission wavelengths, respectively.

The fluorescence intensities were determined at λ_{max}, and data were analyzed using the Stern-Volmer equation (12).

$$\frac{F_o}{F_c} = 1 + K_{SV} \times [NP] \quad \text{(Eq. 2)}$$

Circular dichroism spectroscopy

The far- and near-UV CD spectra ranging from 200–260 and 240–340 nm, respectively, were obtained using a JASCO-810 spectropolarimeter equipped with a thermostatically controlled cell holder. The concentration of CT used for far- and near-UV CD was 3 and 30 μM, respectively, and that of ZnO NP varied from 0 to 15 μg/ml. The final data represents the average

of three scans and a bandwidth of 1 nm. From each sample spectra, contribution of the buffer was subtracted.

Pulldown assay

The CT-induced culture supernatant of O395 and C6706 strains were incubated with ZnO NP for 1 h at room temperature. Cells were centrifuged at 6000 rpm for 10 min at 4 °C followed by washing three times with PBS. The NP-protein pellet was dissolved in Laemmli buffer and boiled for 10 min. Finally, immunoblotting was done using anti-cholera toxin antibody as described before.

Activity assay

For HSA, esterase activity was checked in the presence of ZnO NP (0–25 μg/ml). 1 ml of 1 mg/ml of HSA in 10 mM Tris-Cl, pH 8.0, was incubated with different concentrations of ZnO NP for 1 h. Then 5 μl of 0.1 M *p*-nitrophenyl acetate was added and kept at 22 °C. Finally, absorbance was measured at 400 nm at different time points (14). For the respective ZnO NP concentration, a control sample without albumin was followed in a similar manner to subtract the effect of ZnO NP on *p*-nitrophenyl acetate.

For lysozyme, lysis of *Micrococcus lysodeikticus* cells was monitored to determine its activity (18). 300 units/ml of lysozyme in phosphate buffer, pH 6.2, was incubated with ZnO NP (0–25 μg/ml) for 1 h. These samples were used to monitor the lyses of cells at 450 nm for 5 min. Last, HSP90α activity was determined by measuring the release of inorganic phosphate due to hydrolysis of ATP using a malachite green assay (25).

Gel filtration chromatography

Gel filtration chromatography was used to analyze the effect of ZnO NP on the quaternary structure of CT. Size exclusion high pressure liquid chromatography of CT, CT + ZnO NP (10 μg/ml) was performed with a Polysep-GFC-P 4000 column (300 × 7.8 mm; Phenomenex) equilibrated with 20 mM HEPES, 100 mM NaCl, pH 7.5. For positive control, CT was incubated in 0.1 M glycine-HCl buffer, pH 3.3, containing 3 M urea for 1 h (44).

Cell culture

The human embryonic kidney cell line (HEK293) and human colon adenocarcinoma cell line (HT-29) were purchased from American Type Culture Collection (ATCC HTB-38, Manassas, VA). Cells were grown in Dulbecco's modified Eagle's medium (DMEM, Gibco) supplemented with 1 mM L-glutamine, 10% fetal bovine serum, 50 μg/ml of penicillin, 50 μg/ml of streptomycin, and 2.5 μg/ml of amphotericin B and non-essential amino acids at 37 °C under 5% CO_2. Cells were grown to not more than 80–90% confluence.

HT-29 cell bioassay

1×10^6 HT-29 cells cultured in DMEM were incubated with 20 μg/ml of CT alone or with various concentrations of ZnO NP for 2 h at 37 °C. The morphology of the cells was evaluated by phase-contrast microscopy (Leica DFC450 C, Leica Microsystems India Pvt. Ltd.).

MTT assay

The growth inhibition and lack of metabolic activity of *V. cholerae* strains and HEK293 and HT-29 cell lines were determined using MTT assay. *V. cholerae* and HEK293 cells were grown alone in the presence of different concentrations of ZnO NP for 18 and 48 h, respectively, washed with PBS, and incubated with MTT solution for 2 h at 37 °C. To dissolve formazan crystals, 100 μl of DMSO was added to each well and optical density was monitored at 595 nm.

The percentage of viability was calculated as cytotoxicity (32).

$$\left(1 - \frac{A_{\text{test}}}{A_{\text{control}}}\right) \times 100 \qquad \text{(Eq. 3)}$$

Statistical analysis

Data are represented as the mean ± S.D. All statistical analyses were performed with GraphPad Prism 5 software, using one-way ANOVA followed with Dunnett's multiple comparison test. $p < 0.05$ was considered statistically significant.

Author contributions—S. S. designed and performed the experiments, analyzed the data, and wrote the manuscript. A. A. and M. P. performed cell line experiments and analyzed the data. A. A. also studied the interaction and activity of HSP90α. P. C. designed the experiments, wrote and edited the manuscript, supervised, and directed overall research. All authors reviewed the results and approved the final version of the manuscript.

References

1. World Health Organization. (2016) Cholera, 2015. *Weekly Epidemiological Record.* **91,** 433–440
2. Ali, M., Nelson, A. R., Lopez, A. L., and Sack, D. A. (2015) Updated global burden of cholera in endemic countries. *PLoS Negl. Trop. Dis.* **9,** e0003832
3. Harris, J. B., LaRocque, R. C., Qadri, F., Ryan, E. T., and Calderwood, S. B. (2012) Cholera. *Lancet* **379,** 2466–2476
4. Pang, B., Yan, M., Cui, Z., Ye, X., Diao, B., Ren, Y., Gao, S., Zhang, L., and Kan, B. (2007) Genetic diversity of toxigenic and nontoxigenic Vibrio cholerae serogroups O1 and O139 revealed by array-based comparative genomic hybridization. *J. Bacteriol.* **189,** 4837–4849
5. Siddique, A. K., Nair, G. B., Alam, M., Sack, D. A., Huq, A., Nizam, A., Longini, I. M., Jr., Qadri, F., Faruque, S. M., Colwell, R. R., Ahmed, S., Iqbal, A., Bhuiyan, N. A., and Sack, R. B. (2010) El Tor cholera with severe disease: a new threat to Asia and beyond. *Epidemiol. Infect.* **138,** 347–352
6. Mahamud, A. S., Ahmed, J. A., Nyoka, R., Auko, E., Kahi, V., Ndirangu, J., Nguhi, M., Burton, J. W., Muhindo, B. Z., Breiman, R. F., and Eidex, R. B. (2012) Epidemic cholera in Kakuma Refugee Camp, Kenya, 2009: the importance of sanitation and soap. *J. Infect. Dev. Ctries.* **6,** 234–241
7. Akanda, A. S., Jutla, A. S., Gute, D. M., Sack, R. B., Alam, M., Huq, A., Colwell, R. R., and Islam, S. (2013) Population vulnerability to biannual cholera outbreaks and associated macro-scale drivers in the Bengal delta. *Am. J. Trop. Med. Hyg.* **89,** 950–959
8. Smallman-Raynor, M. R., and Cliff, A. D. (2004) Impact of infectious diseases on war. *Infect. Dis. Clin.* **18,** 341–368
9. Shears, P. (1991) Epidemiology and infection in famine and disasters. *Epidemiol. Infect.* **107,** 241–251
10. Spagnuolo, A. M., Dirita, V., and Kirschner, D. (2011) A model for *Vibrio cholerae* colonization of the human intestine. *J. Theor. Biol.* **289,** 247–258
11. Sánchez, J., and Holmgren, J. (2008) Cholera toxin structure, gene regulation and pathophysiological and immunological aspects. *Cell Mol. Life Sci.* **65,** 1347–1360

12. Lakowicz, J. R. (ed) (2006) Introduction to Fluorescence. in *Principles of Fluorescence Spectroscopy*, pp. 1–26, Springer, Boston, MA
13. Azman, A. S., Lessler, J., Satter, S. M., Mckay, M. V., Khan, A., Ahmed, D., and Gurley, E. S. (2015) Tracking cholera through surveillance of oral rehydration solution sales at pharmacies: insights from urban Bangladesh. *PLoS Negl. Trop. Dis.* **9,** e0004230
14. Lockridge, O., Xue, W., Gaydess, A., Grigoryan, H., Ding, S.-J., Schopfer, L. M., Hinrichs, S. H., and Masson, P. (2008) Pseudo-esterase activity of human albumin: slow turnover on tyrosine 411 and stable acetylation of 82 residues including 59 lysines. *J. Biol. Chem.* **283,** 22582–22590
15. Duggan, C., Fontaine, O., Pierce, N. F., Glass, R. I., Mahalanabis, D., Alam, N. H., Bhan, M. K., and Santosham, M. (2004) Scientific rationale for a change in the composition of oral rehydration solution. *JAMA* **291,** 2628–2631
16. Nelson, E. J., Nelson, D. S., Salam, M. A., and Sack, D. A. (2011) Antibiotics for both moderate and severe cholera. *N. Engl. J. Med.* **364,** 5–7
17. Mandal, J., Dinoop, K. P., and Parija, S. C. (2012) Increasing antimicrobial resistance of *Vibrio cholerae* OI biotype EI Tor strains isolated in a tertiary-care centre in India. *J. Health Popul. Nutr.* **30,** 12–16
18. Shugar, D. (1952) The measurement of lysozyme activity and the ultraviolet inactivation of lysozyme. *Biochim. Biophys. Acta* **8,** 302–309
19. Kitaoka, M., Miyata, S. T., Unterweger, D., and Pukatzki, S. (2011) Antibiotic resistance mechanisms of *Vibrio cholerae*. *J. Med. Microbiol.* **60,** 397–407
20. Rudramurthy, G. R., Swamy, M. K., Sinniah, U. R., and Ghasemzadeh, A. (2016) Nanoparticles: alternatives against drug-resistant pathogenic microbes. *Molecules* **21,** e836
21. Allahverdiyev, A. M., Kon, K. V., Abamor, E. S., Bagirova, M., and Rafailovich, M. (2011) Coping with antibiotic resistance: combining nanoparticles with antibiotics and other antimicrobial agents. *Expert Rev. Anti Infect. Ther.* **9,** 1035–1052
22. Franci, G., Falanga, A., Galdiero, S., Palomba, L., Rai, M., Morelli, G., and Galdiero, M. (2015) Silver nanoparticles as potential antibacterial agents. *Molecules* **20,** 8856–8874
23. Zhao, Y., Tian, Y., Cui, Y., Liu, W., Ma, W., and Jiang, X. (2010) Small molecule-capped gold nanoparticles as potent antibacterial agents that target Gram-negative bacteria. *J. Am. Chem. Soc.* **132,** 12349–12356
24. Lam, S. J., O'Brien-Simpson, N. M., Pantarat, N., Sulistio, A., Wong, E. H., Chen, Y.-Y., Lenzo, J. C., Holden, J. A., Blencowe, A., Reynolds, E. C., and Qiao, G. G. (2016) Combating multidrug-resistant Gram-negative bacteria with structurally nanoengineered antimicrobial peptide polymers. *Nat. Microbiol.* **1,** 16162
25. Nadeau, K., Das, A., and Walsh, C. T. (1993) Hsp90 chaperonins possess ATPase activity and bind heat shock transcription factors and peptidyl prolyl isomerases. *J. Biol. Chem.* **268,** 1479–1487
26. Baqui, A. H., Black, R. E., El Arifeen, S., Yunus, M., Chakraborty, J., Ahmed, S., and Vaughan, J. P. (2002) Effect of zinc supplementation started during diarrhoea on morbidity and mortality in Bangladeshi children: community randomised trial. *BMJ.* **325,** 1059
27. Wadhwa, N., Natchu, U. C., Sommerfelt, H., Strand, T. A., Kapoor, V., Saini, S., Kainth, U., S., and Bhatnagar, S. (2011) ORS containing zinc does not reduce duration or stool volume of acute diarrhea in hospitalized children. *J. Pediatr. Gastroenterol. Nutr.* **53,** 161–167
28. Negi, R., Dewan, P., Shah, D., Das, S., Bhatnagar, S., and Gupta, P. (2015) Oral zinc supplements are ineffective for treating acute dehydrating diarrhoea in 5–12 year olds. *Acta Paediatr.* **104,** e367–e371
29. Seil, J. T., and Webster, T. J. (2012) Antimicrobial applications of nanotechnology: methods and literature. *Int. J. Nanomedicine* **7,** 2767–2781
30. Kołodziejczak-Radzimska, A., and Jesionowski, T. (2014) Zinc oxide: from synthesis to application: a review. *Materials* **7,** 2833–2881
31. Reddy, K. M., Feris, K., Bell, J., Wingett, D. G., Hanley, C., and Punnoose, A. (2007) Selective toxicity of zinc oxide nanoparticles to prokaryotic and eukaryotic systems. *Appl. Phys. Lett.* **90,** 2139021–2139023
32. Sarwar, S., Chakraborti, S., Bera, S., Sheikh, I. A., Hoque, K. M., and Chakrabarti, P. (2016) The antimicrobial activity of ZnO nanoparticles against *Vibrio cholerae*: variation in response depends on biotype. *Nanomedicine* **12,** 1499–1509
33. Childers, B. M., and Klose, K. E. (2007) Regulation of virulence in *Vibrio cholerae*: the ToxR regulon. *Future Microbiol.* **2,** 335–344
34. Mocz, G., and Ross, J. (2013) Fluorescence techniques in analysis of protein–ligand interactions in protein-ligand Interactions. *Methods Mol. Biol.* **1008,** 169–210
35. Greenfield, N. J. (2006) Determination of the folding of proteins as a function of denaturants, osmolytes or ligands using circular dichroism. *Nat. Protoc.* **1,** 2733–2741
36. Benitez, J. A., and Silva, A. J. (2016) *Vibrio cholerae* hemagglutinin(HA)/protease: an extracellular metalloprotease with multiple pathogenic activities. *Toxicon* **115,** 55–62
37. Charania, Z., Vanmaele, R., and Armstrong, G. D. (1991) A bioassay for cholera-like toxins using HT29 cells. *J. Microbiol. Methods* **14,** 171–176
38. De Haan, L., and Hirst, T. R. (2004) Cholera toxin: a paradigm for multifunctional engagement of cellular mechanisms (review). *Mol. Membr. Biol.* **21,** 77–92
39. Hung, D. T., Shakhnovich, E. A., Pierson, E., and Mekalanos, J. J. (2005) Small-molecule inhibitor of *Vibrio cholerae* virulence and intestinal colonization. *Science* **310,** 670–674
40. Shakhnovich, E. A., Hung, D. T., Pierson, E., Lee, K., and Mekalanos, J. J. (2007) Virstatin inhibits dimerization of the transcriptional activator ToxT. *Proc. Natl. Acad. Sci.* **104,** 2372–2377
41. Pariwat, P., Homvisasevongsa, S., Muanprasat, C., and Chatsudthipong, V. (2008) A natural plant-derived dihydroisosteviol prevents cholera toxin-induced intestinal fluid secretion. *J. Pharmacol. Exp. Ther.* **324,** 798–805
42. Chatterjee, S., Asakura, M., Chowdhury, N., Neogi, S. B., Sugimoto, N., Haldar, S., Awasthi, S. P., Hinenoya, A., Aoki, S., and Yamasaki, S. (2010) Capsaicin, a potential inhibitor of cholera toxin production in *Vibrio cholerae*. *FEMS Microbiol. Lett.* **306,** 54–60
43. Chatterjee, T., Chatterjee, B. K., Saha, T., Hoque, K. M., and Chakrabarti, P. (2017) Structure and function of *Vibrio cholerae* accessory cholera enterotoxin in presence of gold nanoparticles: dependence on morphology. *Biochim. Biophys. Acta* **1861,** 977–986
44. Ohtomo, N., Muraoka, T., Tashiro, A., Zinnaka, Y., and Amako, K. (1976) Size and structure of the cholera toxin molecule and its subunits. *J. Infect. Dis.* **133,** 31–40